Effect of Mass Transfer and Catalyst Layer Thickness on Photocatalytic Reaction

Dingwang Chen, Fengmei Li, and Ajay K. Ray
Dept. of Chemical and Environmental Engineering, The National University of Singapore, 10 Kent Ridge Crescent, Singapore 119260

Semiconductor photocatalytic processes have been studied for nearly 20 years due to their intriguing advantages in environmental remediation. A rational approach in determining the effect of mass transfer and catalyst layer thickness during photocatalytic reactions is proposed. The reaction occurs at the liquid–catalyst interface, and therefore when the catalyst is immobilized, both external and internal mass transfer plays significant roles in overall photocatalytic processes. Several model parameters—external mass-transfer coefficient, dynamic adsorption equilibrium constant, adsorption rate constant, internal mass-transfer coefficient, and effective diffusivity—were determined either experimentally or by fitting realistic models to experimental results using benzoic acid as a model component. Even though all these parameters are critical to the design and development of photocatalytic processes, they are not available in the literature. The effect of the internal mass transfer on the photocatalytic degradation rate over different catalyst layer thicknesses under two different operating configurations was analyzed theoretically and experimentally verified. It was observed that an optimal catalyst layer thickness exists for substrate-to-catalyst illumination.

Introduction

It has been demonstrated (Schiavello, 1988; Serpone and Pelizzetti, 1989; Ollis and Al-Ekabi, 1993) that semiconductor photocatalysis has a large number of applications, including destruction of VOCs in air, splitting of water to produce hydrogen, conversion of carbon dioxide into useful hydrocarbon, recovery of noble metals from wastewater, oxidation of liquid hydrocarbons (alkanes, alkenes, cycloalkanes, aromatics) into aldehydes and ketones, transformation of toxic inorganic ions (SO_3^{2-}, S^{2-}, NO_2^- CN^-, and OCN^-) into innocuous ions (SO_4^{2-}, NO_3^-), as well as mineralization of toxic organics in wastewater. In recent years, few review papers (Mills et al., 1993; Legrini et al., 1993; Fox and Dulay, 1993; Hoffmann et al., 1995; Mills and Hunte, 1997) have been published in this field. It has been reported that process efficiency can be competitive with other available treatment technologies at a low organic concentration level for water (Ollis et al., 1989) and air (Miller and Fox, 1993). Compounds reported in the literature, which could be degraded into environmentally acceptable species such as carbon dioxide and mineral acids include phenols, benzenes, chlorinated aromatics, nitrogenous compounds, and pesticides. Many of these species are in the EPA list of priority pollutants.

Among the semiconductor photocatalysts tested, Degussa P25 TiO_2 has been proven to be the most active catalyst (Mills et al., 1993). TiO_2 catalyst has been used in two forms: suspended in aqueous solutions and immobilized onto rigid inert supports. In the former case, a high ratio of illuminated catalyst surface to the effective reactor volume can be achieved for a small, well-designed photocatalytic reactor (Ray and Beenackers, 1997), and almost no mass-transfer limitation exists since the maximum diffusional distance is very small, resulting from the use of ultrafine (< 30 nm) catalyst particles (Chen and Ray, 1998). In large-scale applications, however, the catalyst particles must be filtered prior to the discharge of the treated water, even though TiO_2 is harmless to environment. Hence, a liquid–solid separator must follow the slurry reactor. The installation and operation of such a sepa-

Correspondence concerning this article should be addressed to A. K. Ray.

rator will significantly raise the cost of the overall process, as the separation of the ultrafine catalyst particles is a slow and expensive process. Besides, the penetration depth of UV light is limited due to the strong absorption by TiO_2 and dissolved organic species. All these disadvantages render the scale-up of a slurry photocatalytic reactor very difficult (Mukherjee and Ray, 1999; Ray, 1999).

The preceding problems can be eliminated by immobilizing TiO_2 catalyst over suitable supports (Matthews, 1987; Nogueira and Jardim, 1996; Peill and Hoffman, 1996; Ray and Beenackers, 1996). Design and development of immobilized thin catalyst film makes it possible for commercial-scale applications of TiO_2-based photocatalytic processes for water treatment (Ray and Beenackers, 1996, 1998a, 1998b; Ray, 1999). The designs are more likely to be useful in commercial applications, as the catalyst film provides at least three important advantages. First, it eliminates the need for the separation of catalyst particles from treated liquid and enables the contaminated water to be treated continuously. Second, the catalyst film is porous, and can therefore provide a large surface area for the degradation of contaminant molecules. Third, when a conductive material is used as a support, the catalyst film can be connected to an external potential to remove excited electrons to reduce electron–hole recombination, thereby significantly improving the process efficiency (Vinodgopal et al., 1993; Ichikawa and Doi, 1996). However, immobilization of TiO_2 on supports also creates its own problems (Periyathamby and Ray, 1999). There are at least two obvious problems arising from this arrangement: the accessibility of the catalytic surface to the photons and the reactants, and the significant influence of the external mass transfer particularly at low fluid flow rate, due to the increasing diffusional length of the reactant from the bulk solution to the catalyst surface. While on the other hand, with the increase of catalyst film thickness, the internal mass transfer may play a dominant role by limiting utilization of the catalyst near the support surface due to internal mass-transfer resistance. All these usually lead to a lower overall degradation rate when catalyst is immobilized compared with the suspended system (Matthews, 1992; Matthews and McEvoy, 1992). Surprisingly, there are very few investigations (Sclafani et al., 1993) that offer a rational approach to the study of the influence of mass transfer in immobilized catalyst films, although studies in the photocatalytic field have reached the preindustry stage. The majority of the researchers in this area have focused on the investigation of the effect of operational parameters on the photocatalytic degradation rate, and of the reactor design. Edwards et al. (1996) investigated the effectiveness factor of the photocatalytic reaction in planar membrane under two different illumination configurations. To the best of our knowledge, no other research work on dynamic mass-transfer parameters has been reported in the literature.

In this article, the effect of mass transfer and catalyst layer thickness on photocatalytic degradation of organic pollutant in a TiO_2 immobilized system was investigated. Benzoic acid was chosen as the model compound because of its relatively high adsorptive capacity on Degussa P25 TiO_2. A simple illumination source and reactor geometry were used in order to make it possible to extrapolate the experimental results for large-scale systems. Experiments of physical adsorption and photocatalytic reaction were conducted in the reactor for different catalyst layer thickness. The external mass-transfer coefficient was correlated as a function of the Reynolds' number. The dynamic adsorption equilibrium constant, adsorption rate constant, effective diffusivity of benzoic acid within the porous catalyst layer, and light adsorption coefficient of the P25 TiO_2 were determined by fitting the experimental data to the relevant models. The optimal catalyst layer thickness was obtained under two different illumination modes: the effect of internal mass transfer on the photocatalytic reaction was analyzed, and later internal mass-transfer coefficients were experimentally determined for both operating modes.

Experimental Details

Materials

Degussa P25 catalyst provided by the Degussa Company (Germany) was used throughout this work without further modification. Its main physical data are as follows: BET surface area 55 ± 15 m^2/g; average primary particle size around 30 nm; and purity above 97% and with anatase:rutile, 80:20. Benzoic acid (99.5 + %) was obtained from BDH Chemicals, nitric acid (65% by weight) from Merck Chemicals, sodium hydroxide (98 + %) from Baker Chemicals, and acetonitrile (for HPLC) from Fisher. All chemicals were used as received. Water used in this work was always Milli-Q water.

Apparatus and analyses

The semibatch photoreactor consisted of two circular glass plates that were placed between soft padding housed within stainless-steel and aluminum casings. The TiO_2 catalyst was coated either on the top surface of the bottom glass plate or on the bottom surface of the top one. The reaction solution, which was circulated by a peristaltic pump, was introduced tangentially between the two glass plates, and exited from the center of the top plate. The tangential introduction of liquid created a swirl-flow, thereby ensuring that the liquid solution was well mixed (Ray and Beenackers, 1997). Two reactors with the same configuration but different dimensions were used in this study. Dynamic physical adsorption experiments were conducted in reactor 1 ($V = 1.88 \times 10^{-5}$ m^3, $d = 0.073$ m), which had a high specific mass transfer area. This reactor was connected to a Perkin-Elmer UV spectrophotometer for on-line measurement of benzoic acid. The second reactor, reactor 2 ($V = 3.8 \times 10^{-5}$ m^3, $d = 0.05$ m), was used for the photocatalytic reaction experiments. A lamp (Philips HPR 125-W high-pressure mercury vapor) was placed about 0.1 m underneath the bottom glass plate on a holder that could be moved to create a different angle of incidence of light. The lamp has a spectral energy distribution with a sharp (primary) peak at $\lambda = 365$ nm of 2.1 W, and thus the incident light intensity was 213 W/m^2. The lamp and reactor were placed inside a wooden box painted black so that no stray light could enter the reactor. The lamp was constantly cooled by compressed air to keep the temperature down, thereby protecting the lamp from overheating.

A Shimadzu 5000A TOC analyzer with an ASI-5000 autosampler was used to analyze the TOC in the samples. The concentration of benzoic acid in the reaction samples was analyzed by a HPLC (Perkin-Elmer LC240). Aliquots of 20 μL

were injected onto a reverse-phase C-18 column (Chrompack), and eluted with the mixture of acetonitrile (60%) and ultrapure water (40%) at a total flow rate of 1.5 mL/min. Absorbance at 229 nm was used to measure the concentration of the preceding compounds by a UV/VIS detector (Perkin-Elmer 785A). All water samples were filtered by a Millex-HA filter (Millipore, 0.45 μm) before analysis. The light intensity was measured by a digital radiometer (UVP Model number UVX-36).

Catalyst support and immobilization

In heterogeneous photocatalysis, the primary role of a catalyst support is to provide, on its external surface, strong adherence of the photocatalyst. Catalyst supports studied in the literature fall into two categories, transparent and nontransparent materials. Glass is one of the transport materials, and it has been extensively used in laboratory studies. A variety of support configurations have been investigated in the literature, such as beads (Serpone et al., 1986), tubes (Chester et al., 1993), plates (Sabate et al., 1991), and fibers (Zhang et al., 1994). The adhesion of TiO_2 on Pyrex glass support was strong since no significant detachment of TiO_2 was observed if the coated film was well-processed. The strong adhesion is usually achieved by making the support surface rough (through sandblasting) and afterwards, heat treatment of the catalyst-coated support. Sand (Zhang et al., 1994), stainless steel (Fernandez et al., 1995), and organic membrane (Tennakone and Kottegoda, 1996) are the literature-reported nontransparent materials used as support. Recently, adsorbents such as zeolite, silica, and activated carbon have also been used as support (Torimoto et al., 1996).

In this study, circular Pyrex glass (thickness 0.0032 m) was used as catalyst support. Pyrex glass provides several advantages, namely, it can cut off UV light below 300 nm, thereby eliminating direct photolysis of the organic compounds, it is cheaper (compared to quartz), and adhesion of TiO_2 coatings is stronger (than quartz); Pyrex therefore has more potential as a support for commercial applications.

There are mainly two successful methods for the immobilization of catalyst on inert supports: (1) preparation of a catalyst *in situ* from a precursor (Hofstadler et al., 1994; Bideau et al., 1995), and (2) coating using commercially available TiO_2 directly by the dip-coating technique (Haarstrick et al., 1996; Lu et al., 1993). In the present study, the second method was adopted. A 5 wt % solution of Degussa P25 TiO_2 was prepared in an ultrasonic cleaner bath for one hour to obtain a stable milky suspension. The glass plate was cleaned with alkaline solution followed by acid solution overnight to remove impurities, washed with Millipore Milli-Q water, and finally dried at 393 K for 2 h before coating. The glass plate was then coated with catalyst by dipping into the suspension and pulling out slowly by the dip-coating technique. The coated catalyst was dried at 393 K for one half-hour. This procedure was repeated up to 15 times depending on the desired amount of coated catalyst. Varied catalyst film thickness was obtained by controlling the speed of coating and the number of times coated using an automated dip-coating apparatus (Ray and Beenackers, 1998a). Subsequently, the coated glass plate was calcined in a furnace by raising the temperature gradually at a rate of 5 K/min to a final temperature of 573 K, held there for 3 h, and finally, cooled down using the same ramping rate until it reached room temperature. Gradual heating and cooling is necessary, as otherwise the catalyst film might crack. Afterwards, the coated catalyst film was brushed gently and flushed with water to remove the loosely bound catalyst particles. The total mass of catalyst deposited per unit area was determined by weighing the glass plate before and after the catalyst coating. Subsequently, catalyst layer thickness was calculated based on the density of the catalyst particles and layer porosity. The surface texture measurement of the coated catalyst layer by Taylor-Hobson indicated that catalyst particles were uniformly distributed on the whole glass plate. Scanning electron micrograph pictures illustrating the surface morphology of a roughened (sandblasted) glass plate with no catalyst, and TiO_2 films containing 5.0×10^{-4} kg/m^2 (thin film) and 3.0×10^{-3} kg/m^2 (thick film) have been published elsewhere (Ray and Beenackers, 1997). The coated catalyst was observed to be stable for a wide range of pH. The TiO_2 immobilized in this way was found to be photocatalytically active, capable of decomposing a variety of organic substances, including phenol, 4-chlorophenol, 4-nitrophenol, and benzoic acid (Chen and Ray, 1998, 1999). In this work, we focused on the photocatalytic degradation of benzoic acid.

Adherence of photocatalyst to its support is rarely reported in the literature, although it is of paramount importance, since, if it is not strong enough, some of the catalyst particles will be lost. In the present study, experimental results demonstrated loss of an observable amount of catalyst when the catalyst/substrate was calcined at low temperature (less than 473 K). On the other hand, when calcined at high temperature, appreciable loss of catalyst activity presumably due to the increase of internal mass-transfer resistance, is observed. The influence of the calcination temperature on the reactivity of the immobilized catalyst layer was reported in one of our earlier articles (Chen and Ray, 1999). The optimal calcination temperature found out was around 573 K.

Results and Discussion

Concentration and light-intensity profiles

Experiments were performed to study the photocatalytic degradation rate when catalyst was immobilized either on the bottom plate or on the top plate. In the latter case, light intensity falling on the catalyst surface will be considerably reduced, as it will have to travel through the absorbing liquid medium. The two circumstances can be depicted as substrate-catalyst (SC) and liquid-catalyst (LC) illumination, depending on whether the catalyst is activated from the substrate side or from the liquid side. Figure 1 shows where the porous TiO_2 catalyst layer is coated on the left side of an inert support (Pyrex glass). The UV light source can be positioned either on the left (LC illumination) or on the right (SC illumination) side of the glass plate. Accordingly, Figures 1a and 1b represent the cases in which the catalyst-coated glass plate is placed at the top (LC illumination) or at the bottom (SC illumination), respectively, for the photocatalytic reactor used in this work.

A sequence of events can be postulated for photocatalytic degradation of benzoic acid within the porous catalyst film. Benzoic acid must diffuse from the bulk liquid through a boundary layer to reach the liquid–catalyst interface, that is,

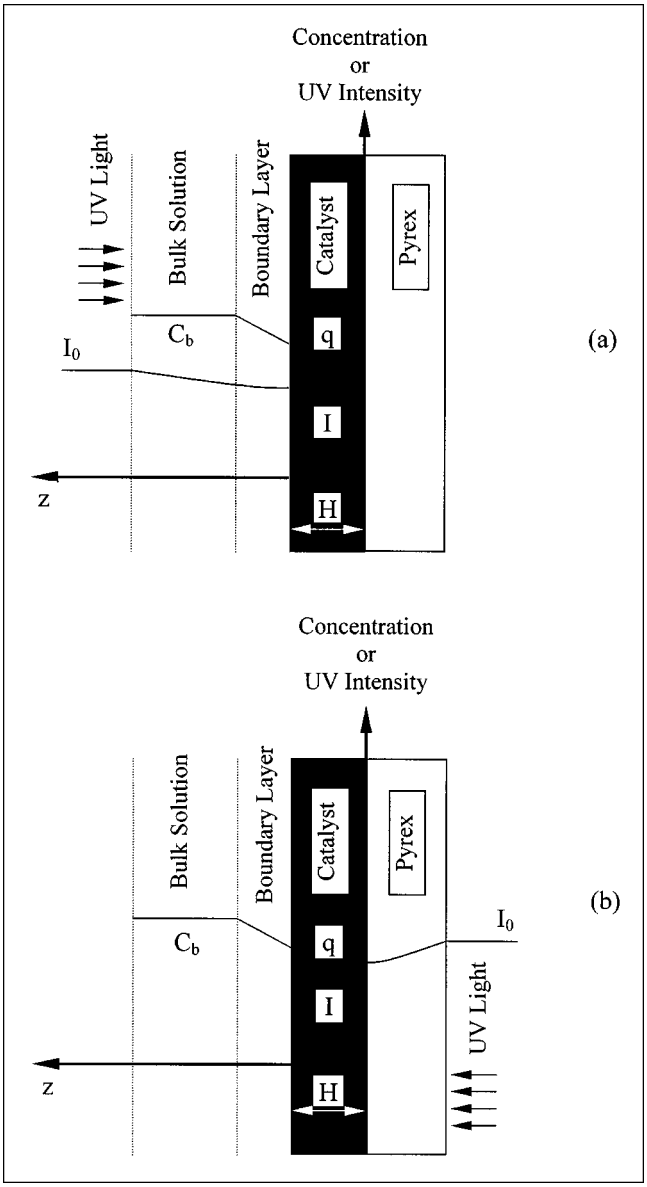

Figure 1. Profiles of concentration and UV intensity in TiO_2 immobilized system: (a) LC illumination; (b) SC illumination.

liquid–film mass transfer. Benzoic acid must then migrate through the catalyst layers (interparticle diffusion within the film) to find active surface sites where it adsorbs and eventually reacts. The mass-transfer process through the layer is similar to interparticle diffusion and is defined as an internal mass-transfer process. It should be noted that TiO_2 catalyst particles are nonporous, and therefore intraparticle diffusion is absent. Simultaneous to the mass transport of organic molecules, UV light must also reach the catalyst surface. Unless light reaches the catalyst surface, the catalyst does not show any catalytic power for photocatalytic degradation. The depth of UV light penetration within the catalyst depends on the optical properties of the catalyst layers and the brand of catalyst. The light intensity decreases with the depth of penetration due to the strong absorption of light by the catalyst.

Figure 1 illustrates the concentration profile of benzoic acid and the intensity profile of UV light based on the sequence of events described earlier. Evidently, the profile of light intensity will be quite different from that of the concentration profile of benzoic acid. Unlike the presence of mass-transfer resistance at the solid–liquid interface, there is no boundary-layer resistance for the UV penetration, and the decrease in light intensity in the liquid phase results only from the absorption of light by the solution. Hence, there is no *jump* in UV light intensity at the liquid–catalyst interface. In order to facilitate the quantitative description of the two profiles, a Cartesian coordinate is defined as shown in the figure. The origin ($z = 0$) is located at the catalyst–substrate interface, and the distance z increases toward the bulk liquid solution.

As described earlier, in the photocatalytic reaction over the immobilized catalyst, both internal and external mass transfer must be considered. The relationship among the observed degradation rate, the external and internal mass-transfer rates, and the intrinsic kinetic reaction rate are given by the following expression:

$$\frac{1}{k_{\text{obs}}} = \frac{1}{k_{rxn}} + \frac{1}{k_{m,\text{int}}} + \frac{1}{k_{m,\text{ext}}}. \tag{1}$$

The external mass-transfer resistance can be reduced to a negligible value by increasing the fluid mixing by stirring or increasing the circulating flow rate (Reynolds number) of the reaction medium. The kinetic reaction rate, k_{rxn} can also be increased by increasing the light intensity. However the internal mass transfer is an intrinsic property of the catalyst film and determined by the nature of the catalyst and the coating techniques used and are difficult to alter.

Influence of external mass transfer

In determining the intrinsic kinetic parameters, it is essential to estimate the external mass-transfer resistance. At steady state, the mass-transfer rate to the catalyst surface, $r_{m,\text{ext}}$, must be equal to the surface catalyzed reaction rate, r_{rxn}. The rates $r_{m,\text{ext}}$ and r_{rxn} are given by

$$r_{m,\text{ext}} = k_{m,\text{ext}}(C_b - C_S) \tag{2}$$

$$r_{rxn} = k_{rxn} f(C_S) \tag{3}$$

where $f(C_S)$ represents the concentration dependence of the surface catalyzed reaction rate.

The external mass-transfer coefficient, $k_{m,\text{ext}}$, was determined experimentally by measuring the dissolution rate of benzoic acid into water flowing at different flow rates ($C_{\text{out}}/C_{\text{sat}} \approx 0.04$). The benzoic acid was coated on the inside of the bottom glass plate by the dissolution–evaporation technique using alcohol as the solvent. The result is shown as a function of Reynolds number in Figure 2 together with the best least-square fit, which is correlated by Eq. 4:

$$k_{m,\text{ext}}(\text{in m/s}) = 3.49 \times 10^{-7}\, Re^{0.77} \tag{4}$$

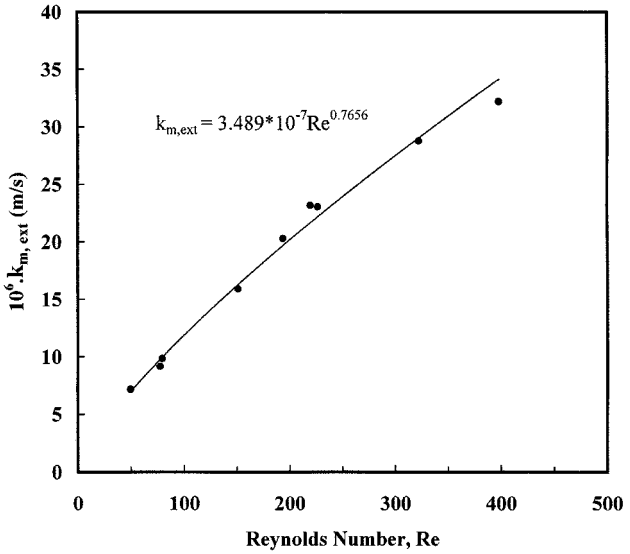

Figure 2. Measurement of external mass-transfer coefficient, $k_{m,ext}$, with Reynolds number.

In this equation, the Reynolds number was calculated based on the equivalent hydraulic diameter of the reactor. The influence of the external mass transfer through the circulating flow rate is also reflected in the dynamic physical adsorption. Figure 3 shows the experimental results for the variation of the benzoic acid concentration with adsorption time (dark or no reaction) at different circulating flow rates. The dimensionless concentration used is defined in the next subsection. Evidently, a decrease in benzoic acid concentration in the bulk solution was observed, and the rate of adsorption increased with the increasing flow rate. However, an almost identical final concentration (equilibrium concentration) was obtained for all flow rates. This indicates that the mass-transfer coefficient increased (less mass-transfer resistance) with increasing circulating flow rate.

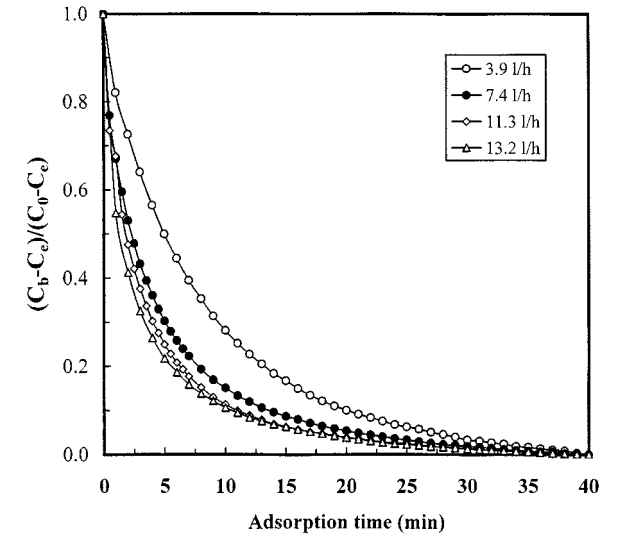

Figure 3. Influence of circulating flow rate on the physical adsorption rate.

Experimental conditions: $m = 8.1\times10^{-5}$ kg; $\nu = 3.5\times10^{-5}$ m^3; $A = 4.17\times10^{-3}$ m^2; $T = 300$ K.

Influence of internal mass transfer

In a heterogeneous photocatalytic system, the internal mass-transfer resistance results from the diffusion of organic molecules within the porous catalyst thin film. The influence of the internal mass transfer on the observed photocatalytic degradation rate can be determined by the magnitude of the Thiele modulus (Froment and Bischoff, 1990). In this study, the thin catalyst film was considered a porous slab. For the first-order reaction, the Thiele modulus is defined as:

$$\phi_H = H\sqrt{\frac{k_\nu}{D_e}}\,, \tag{5}$$

where H is the thickness of the catalyst film, k_ν is the first-order kinetic rate constant, and D_e is the effective diffusivity of the organic molecules within the catalyst film. Rate constant k_ν can be determined experimentally by kinetic study at high circulating flow rate over a monolayer of catalyst film. Evidently, effective diffusivity dominates the internal mass-transfer process. However, no value of effective diffusivity has been reported in the literature for organic compounds in porous TiO_2 film. Hence, in this study, based on the physical adsorption model of benzoic acid in porous catalyst film, the effective diffusivity was determined by best fitting the experimental results to the model equation.

Determination of Adsorption Rate Constant, K. In order to obtain the effective diffusivity, the adsorption rate constant, K, first needs to be determined by performing the dynamic physical adsorption experiments. The thinnest catalyst film (about 0.63 μm) was used so that the internal mass-transfer resistance can be assumed to be negligible. The physical adsorption (dark reaction) process of benzoic acid over a thin TiO_2 catalyst film can be described by the following equations:

$$\nu\frac{dC_b}{dt} = -k_{m,ext}A(C_b - C_S) \tag{6}$$

$$\frac{dq}{dt} = K\left[\frac{k_a q_s C_S}{1+k_a C_S} - q\right] \tag{7}$$

$$\nu(C_0 - C_b) = mq, \tag{8}$$

where C_0 is the initial concentration of benzoic acid (mol/m^3); C_b and C_S are the benzoic acid concentration in the bulk liquid and on the catalyst surface (mol/m^3), respectively; A is the surface area of catalyst film (m^2); ν is the liquid volume used (m^3); q is the concentration of pollutant adsorbed (mol/kg); q_S is the saturated adsorption capacity (mol/kg) when a complete monolayer coverage is achieved; k_a is the Langmuir adsorption coefficient (m^3/mol); K is the adsorption rate constant (l/s); and m is the catalyst mass (kg). In Eq. 7, an extensively used Langmuir isotherm is adopted to describe the adsorption of pollutants on the catalyst (Ollis et al., 1991). The value of $k_a q_S$ was determined from dy-

namic physical adsorption equilibrium experiments with different initial concentrations of benzoic acid. At low pollutant concentration, $k_a C_S \ll 1$, and Eq. 7 reduces to:

$$\frac{dq}{dt} = K(k_a q_S C_S - q). \tag{9}$$

Rearranging Eqs. 6–9, the variation of the bulk concentration of benzoic acid with adsorption time is given by

$$\left[\frac{1}{k_{m,\text{ext}}A} + \frac{1}{k_a K m q_S}\right]\frac{dC_b}{dt} = -\left[\frac{1}{\nu} + \frac{1}{k_a m q_S}\right]C_b + \frac{1}{k_a m q_S}C_0. \tag{10}$$

The analytical solution to Eq. 10 is given by

$$C_b = \frac{C_0}{\nu + m k_a q_S} \times \left\{\nu + m k_a q_S \exp\left[-\frac{k_{m,\text{ext}} AK(\nu + m k_a q_S)}{\nu(k_{m,\text{ext}} A + m k_a q_S K)}t\right]\right\}. \tag{11}$$

In order to obtain a reliable value of K, dynamic physical adsorption experiments were performed for different initial concentrations. If we define a dimensionless concentration,

$$\left[\frac{C_b - C_e}{C_0 - C_e}\right]$$

where C_e is the equilibrium concentration, then Eq. 11 rearranges to

$$\frac{C_b - C_e}{C_0 - C_e} = \exp\left[-\frac{k_{m,\text{ext}} AK(\nu + m k_a q_S)}{\nu(k_{m,\text{ext}} A + m k_a q_S K)}t\right]. \tag{12}$$

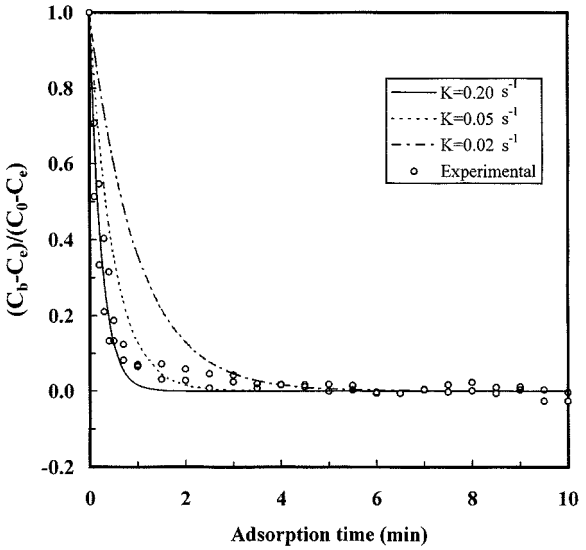

Figure 4. Determination of adsorption rate constant, K.

Experimental conditions: $m = 6.6\times10^{-6}$ kg; $\nu = 3.4\times10^{-5}$ m^3; $k_a q_s = 0.0967$ m^3/kg; $Re = 141$; $A = 4.17\times10^{-3}$ m^2; $T = 300$ K.

Figure 4 shows the experimental results of the dimensionless concentration with adsorption time alongside the effect of fitted adsorption rate constant values. Clearly, a better-fitted value of the adsorption rate constant was obtained with a higher value of K, which decreases the adsorption resistance. The optimum adsorption rate constant, K, obtained by best fitting the experimental results to Eq. 12 is 0.2 s^{-1}.

Determination of Effective Diffusivity. Dynamic physical adsorption experiments over a thicker (about 5.3 μm) catalyst layer were performed for three different initial concentrations of benzoic acid in order to determine the effective diffusivity. It was assumed that the porous catalyst layer is completely wetted by the solution, and all active catalyst sites are equally accessible to the organic pollutant. Pollutant concentrations in the solution and within the porous catalyst layer are a function of both time and position, since dynamic physical adsorption of the pollutant in the catalyst film is an unsteady-state process. The process can be described by the following equations:

$$\epsilon\frac{\partial C_p}{\partial t} = D_e\frac{\partial^2 C_p}{\partial z^2} - \rho_p(1-\epsilon)\frac{\partial q}{\partial t} \tag{13}$$

$$\nu(C_0 - C_b) = \frac{m}{H}\int_0^H q\,dz \tag{14}$$

$$\frac{\partial q}{\partial t} = K(q_S - q), \tag{15}$$

with the boundary and initial conditions as follows:

$$\text{BC:}\quad k_{m,\text{ext}}(C_b - C_p) = D_e\frac{\partial C_p}{\partial z} \quad \text{at } z = 0 \text{ and } t > 0 \tag{16}$$

$$\frac{\partial C_p}{\partial z} = 0 \quad \text{at } z = H \text{ and } t > 0 \tag{17}$$

$$\text{IC:}\quad q = 0 \quad \text{at } t = 0 \tag{18}$$

$$C_p = 0 \quad \text{at } t = 0 \tag{19}$$

$$C_b = C_0 \quad \text{at } t = 0, \tag{20}$$

where C_p is the concentration of benzoic acid inside the catalyst film, C_0 is the initial concentration (mol/m^3), D_e is the effective diffusivity (m^2/s), and ϵ is the porosity of the catalyst layer taken as 0.34 (Vinodgopal et al., 1993). The preceding partial differential equations were solved numerically using the control-volume-based finite difference method (Patankar, 1980). The governing equations were discretized and subsequently solved using the SIMPLER (Patankar, 1980) algorithm with an iterative line-by-line matrix solver. In the present study, the effective diffusivity of benzoic acid in Degussa P25 catalyst was determined by fitting the experimental data to the solution of the preceding model. The model predicts a decreasing rate of dimensionless concentration with the increase of the effective diffusivity (due to the decrease

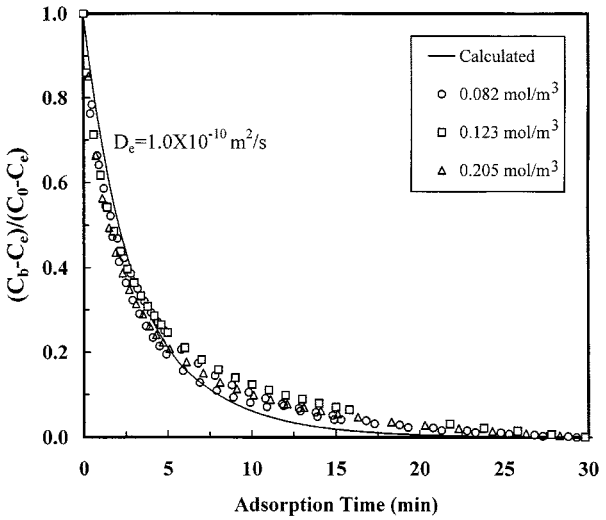

Figure 5. Determination of effective diffusivity of benzoic acid in TiO_2 catalyst film.

Experimental conditions: $\nu = 3.2\times10^{-5}$ m^3; $m = 5.51\times10^{-5}$ kg; $K = 0.2$ s^{-1}; $\epsilon = 0.34$; $\rho_p = 3{,}800$ kg/m^3; $H = 5.27\times10^{-6}$ m; $Re = 141$; $T = 300$ K.

of internal mass-transfer resistance). The result is shown in Figure 5, and a good agreement with the experimental result was obtained when D_e was assumed in the model to be 1.0×10^{-10} m^2/s. The effective diffusivity value obtained is only about one order of magnitude lower than the diffusivity of organics in water (1×10^{-9} m^2/s). However, it should be noted that mass transfer in the bulk (external mass-transfer resistance) can be significantly enhanced by means of agitation (through stirring) or mixing (through turbulence) by increasing flow rate. Internal mass transfer, on the other hand, is controlled by the effective diffusivity and is difficult to modify.

Photocatalytic degradation

It has been well established that when TiO_2 is illuminated by light of wavelength less than 380 nm in the presence of water containing dissolved organic compounds and oxygen, photocatalytic reactions take place (Mills et al., 1993; Legrini et al., 1993; Hoffmann et al., 1995). Photocatalytic reactions proceed through the following steps: (1) generation of electron–hole pairs by absorption of light of suitable energy; (2) generation of space-charge layers owing to the separation of electrons and holes by traps available on the semiconductor surface; (3) redox processes induced at the interface between a bulk semiconductor and a liquid medium by the local electrostatic field present in the space-charge layer with the surface adsorbed species acting as an electron donor or an acceptor. The transfer of mobile charge carriers between the semiconductor and the redox couple thereby generates an electric field within the semiconductor. Two key processes dictate the overall efficiency for interfacial charge transfer. First, there is competition between electron (e^-)/hole (h^+) recombination and trapping, which is followed by the competition between trapped electron–hole recombination and interfacial charge-transfer processes. When the illuminated semiconductor is in contact with a redox couple, an energy equilibrium is set in which the Fermi levels of the semiconductor and the electrochemical potential of the redox couple are adjusted. For an n-type material (TiO_2), the direction of the electric field is such that holes migrate to the surface, where they undergo a chemical reaction, while the electrons create within the film a gradient in the electrochemical potential. Hence, the charge separation does not depend on the Schottky barrier, but is essentially determined by the kinetics at the solid–liquid interface.

The photocatalytic process can be outlined by the following reactions:

$$TiO_2 \xrightarrow{h\nu} TiO_2(h^+ + e^-) \tag{21}$$

$$O_2 + e^- \longrightarrow O_2^{\cdot -} \tag{22}$$

$$OH^- + h^+ \longrightarrow OH^{\cdot} \tag{23}$$

$$OH^{\cdot} + RH \longrightarrow R^{\cdot} + H_2O \longrightarrow CO_2 + H_2O + \text{mineral acid}, \tag{24}$$

where RH represents the organic compound to be degraded. The concentration of hole (h^+) in illuminated TiO_2 particles depends on the incident light intensity and can be described as:

$$C_h = k_I I^a \tag{25}$$

where k_I and a are constants in which the value of a is usually between 0.5 and 1.0 (Chen and Ray, 1998). Therefore, the degradation rate, r_p, of a dissolved organic species on a single illuminated TiO_2 particle is given by

$$r_p = k_d S_p C_S C_h, \tag{26}$$

where k_d is the rate constant, while S_p is the surface area of a single catalyst particle. If ν_p is the volume of a single catalyst particle, then the number of particles in the unit volume of the catalyst layer is $(1-\epsilon)/\nu_p$, and consequently, the total degradation rate, r_t, for a catalyst layer with illuminated surface area, A, thickness, H, can be determined by integrating Eq. 26 over the catalyst volume, AH, and is given by

$$r_t = \nu\frac{dC_b}{dt} = k_I k_d S_p \frac{1-\epsilon}{\nu_p}\int_0^H\int_0^R r\int_0^{2\pi} C_S I^a d\theta\, dr\, dz$$

$$= K_d A(1-\epsilon)\int_0^H C_S I^a dz, \tag{27}$$

where $K_d = k_I k_d S_p/\nu_p$ and $A = \pi R^2$. It should be noted that K_d contains parameters relating to the primary catalyst particles, and therefore K_d is independent of whether the particles are immobilized or suspended. It was also assumed that C_S and I were independent of θ and r; therefore, the integration over these coordinates was simply given by the surface area, A, of the catalyst film in the photocatalytic reactor.

There are two likely loss mechanisms within the films due to the increase in the catalyst layer thickness that will restrict

the presence of charge carriers at the interface. One is attenuation of light due to the absorption by the catalyst, and the other is the increased probability of charge-carrier recombination, presumably because of the increased diffusional lengths through the grain boundaries and constrictions within the microporous film. Three additional assumptions were made for the catalyst film: (1) light propagation inside the porous catalyst layer is through a homogeneous medium; (2) the illuminating light is monochromatic with wavelength λ ($\lambda = 0.365$ μm in this study); and (3) the surface of catalyst film is uniformly illuminated with incident light intensity, I_0. Within the bulk of the catalyst film, the extinction of light follows the exponential principle:

$$I = I_o \exp(-\alpha z), \tag{28}$$

where z is the penetration depth of light within the microporous semiconductor film, and I_0 is the incident light intensity impinging on the surface of catalyst film, that is, $z = H$ (LC illumination) and $z = 0$ (SC illumination), respectively, for Figures 1a and 1b. For simplicity, the light intensity decrease in the liquid and within the glass plate is neglected. The light absorption coefficient, α, is a strong function of wavelength and is approximated (Sodergren et al., 1994) for TiO_2 by

$$\alpha(\mu\text{m}^{-1}) = \exp[29 - 85\lambda\,(\mu\text{m})]. \tag{29}$$

Therefore, α for the incident light of wavelength 365 nm has a value of 0.132 μm^{-1} (6.05 μm^{-1} at 320 nm) and its intensity is attenuated to 10% of its incident value after traversing a distance of 17.4 μm (0.38 μm at 320 nm). Moreover, α is a strong function of λ. Its value varies from 33 μm^{-1} at 0.30 μm to 0.037 μm^{-1} at 0.38 μm.

In the present study, α was determined experimentally (Ray, 1999) by measuring the transmitted UV light intensity at 365 nm for different catalyst layer thicknesses. The experimentally measured value and the least-square fitted line when correlated by Eq. (28) is shown in Figure 6. The value of α obtained was 0.6264 μm^{-1}. Obviously, this value is much larger than the value (0.132 μm^{-1}) calculated by Eq. 29, as the measured α was a bulk parameter that includes the light-scattering effect. Under this circumstance, 95% of the incident light will be absorbed by a catalyst layer of thickness of about 4.8 μm.

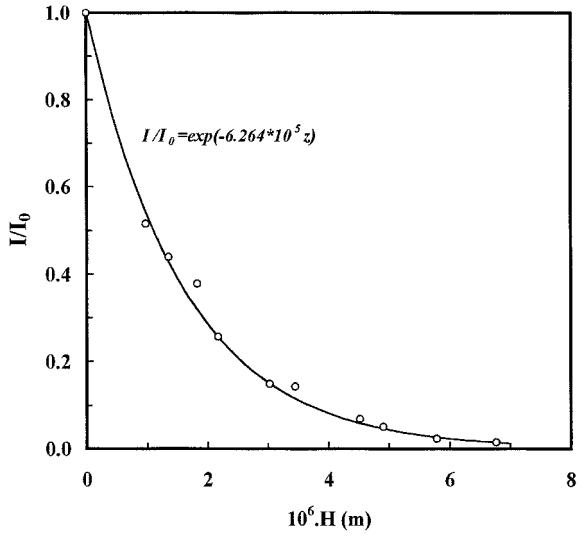

Figure 6. Determination of light absorption coefficient, α, for Degussa P25 TiO_2.

Effect of Catalyst Layer Thickness on Photocatalytic Degradation Rate. It is assumed that the concentration of the pollutant with the catalyst pores decreases exponentially with the effective diffusional length and is described by the following equation:

$$C_S = C_b \exp\left[-\frac{k_f}{D_e}(H - z)\right] \tag{30}$$

where k_f (m/s) is defined as the internal mass-transfer resistance factor.

LC Illumination. When light is introduced from the liquid to the catalyst side (Figure 1a), Eq. 28 becomes

$$I = I_0 \exp[-\alpha(H - z)]. \tag{31}$$

Integrating Eq. 27 by substituting Eqs. 30 and 31, we get

$$r_t = \nu\frac{dC_b}{dt} = \frac{K_d A(1-\epsilon)}{a\alpha + \dfrac{k_f}{D_e}} I_0^a C_b \left\{1 - \exp\left[-\left(a\alpha + \frac{k_f}{D_e}\right)H\right]\right\}. \tag{32}$$

Equation 32 indicates that the photocatalytic rate reaches a saturation value as the catalyst layer thickness increases. This can be understood if we look at the physical problem. When the catalyst film is thin, the absorption of light will not be strong enough, as the wavelength of the light ($\lambda = 0.365$ μm) is of the same order of magnitude as that of the film thickness; consequently, the catalyst layer will not be active to its highest possible level. As the film thickness increases, at some point, light will be completely absorbed by the catalyst layer, and the photocatalytic reaction rate will be at maximum. With further increase in the film thickness, the rate would remain constant, as the diffusional length of the charge carrier to the catalyst–liquid interface will not change.

In order to facilitate the analysis of the effect of the internal mass-transfer factor on the photocatalytic reaction rate, an ideal maximum reaction rate is defined at which the internal mass-transfer resistance factor, k_f, is zero and catalyst layer thickness, H, is infinite. Accordingly, the maximum reaction rate is given by

$$r_{\max} = \frac{K_d A(1-\epsilon)}{a\alpha} I_0^a C_b. \tag{33}$$

Therefore,

$$\frac{r_t}{r_{\max}} = \left[\frac{1}{1 + \dfrac{k_f}{a\alpha D_e}}\right]\left[1 - \exp\left\{-\left(a\alpha + \frac{k_f}{D_e}\right)H\right\}\right]. \tag{34}$$

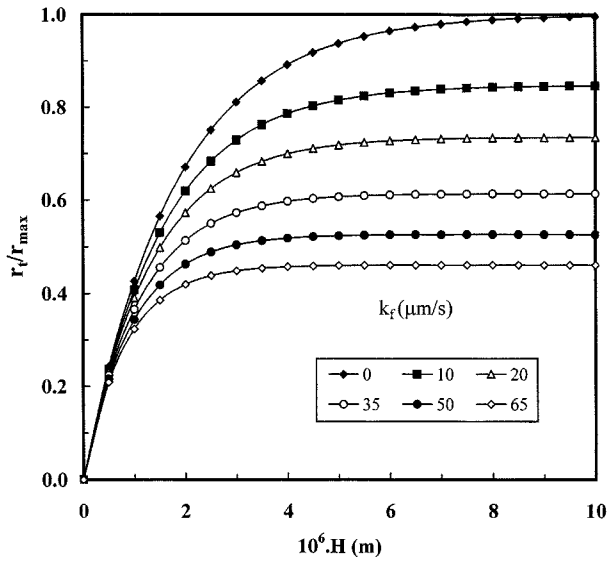

Figure 7. Influence of internal mass transfer on photocatalytic reaction rate for LC illumination.

Experimental conditions: $a = 0.89$; $\alpha = 6.264 \times 10^5$ m^{-1}; $D_e = 1.0 \times 10^{-10}$ m^2/s.

Figure 7 shows the effect of the internal mass-transfer resistance factor on the degradation rate for different catalyst layer thicknesses. Obviously, with the increase of k_f, the reaction rate decreases significantly, particularly when the catalyst film is thick.

SC Illumination. In this case, the catalyst coated glass plate (Figure 1b) is mounted at the bottom of the photoreactor and light is introduced from the substrate to the catalyst film. Integrating Eq. 27 with Eqs. 28 and 30, we get

$$r_t = \nu \frac{dC_b}{dt} = \frac{K_d A(1-\epsilon)}{\dfrac{k_f}{D_e} - a\alpha} I_0^a C_b \times \left[\exp(-a\alpha H) - \exp\left(-H\frac{k_f}{D_e}\right)\right]. \quad (35)$$

Contrary to Eq. 32, Eq. 35 indicates that an optimum catalyst layer thickness exists at which the degradation rate is maximum. The optimum thickness is obtained by equating $dr_t/dH = 0$, and is given by

$$H_{\text{opt}} = \frac{\ln\left[\dfrac{a\alpha D_e}{k_f}\right]}{\left[a\alpha - \dfrac{k_f}{D_e}\right]}. \quad (36)$$

These results can also be explained by the same physical argument as before. Looking first at the thin film, the absorption of the light will not be strong enough, as the wavelength of the light is of the same order of dimension of the film; consequently the catalyst layers in contact with the liquid will not be active to its highest possible level. As the film thickness increases, at some point the pentration depth of the light will be such that most of the electrons and holes will be generated relatively close to the solid–liquid interface. The photocatalytic reaction rate will be about maximum at this point. With a further increase in the film thickness (thicker film), the charge carriers will be generated relatively far from the liquid–catalyst interface; consequently, it will be more susceptible to recombination loss. For SC illumination, a further increase in film thickness will lower the photocatalytic reaction rate, as the charge carrier will now have to diffuse through an increasing number of grain boundaries. This is in contrast with LC illumination, where the rate remains constant, as the diffusional length of charge carriers to the interface does not change. Hence, there exists an *optimal film thickness* for SC illumination for particular values of λ and α at which the photocatalytic reaction rate is at maximum. The expected behavior based on the model is indeed exhibited by the experimental results shown in Figures 8 and 9.

For SC illumination, the $r_{\max}$ expression (similar to the LC illumination case) can be obtained and the dimensionless rate is given by

$$\frac{r_t}{r_{\max}} = \frac{1}{\dfrac{k_f}{a\alpha D_e} - 1}\left[\exp(-a\alpha H) - \exp\left(-H\frac{k_f}{D_e}\right)\right]. \quad (37)$$

The effect of the k_f value on the photocatalytic degradation rate is shown in Figure 10. As in case 1 (LC illumination), k_f has a negative effect on the reaction rate. As expected, Figure 10 shows that an optimum catalyst layer thickness exists, and the optimum catalyst layer thickness decreases with the increase of k_f.

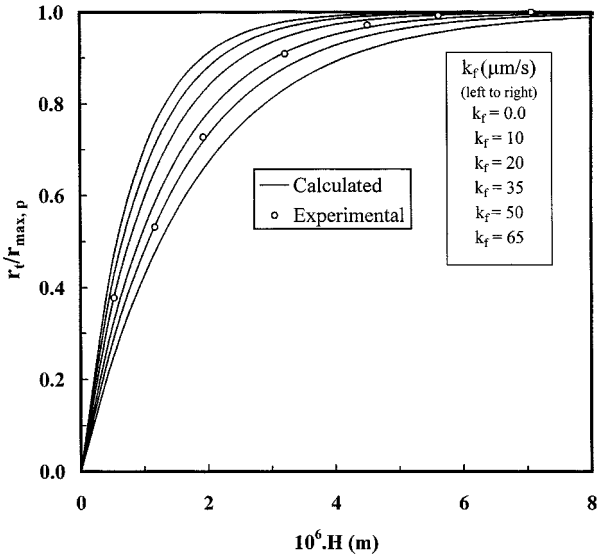

Figure 8. Experimental determination of k_f for LC illumination.

Experimental conditions: $a = 0.89$; $\alpha = 6.264 \times 10^5$ m^{-1}; $D_e = 1.0 \times 10^{-10}$ m^2/s; $A = 0.002$ m^2; $T = 303$ K; $\nu = 1.45 \times 10^{-4}$ m^3; $Re = 427$.

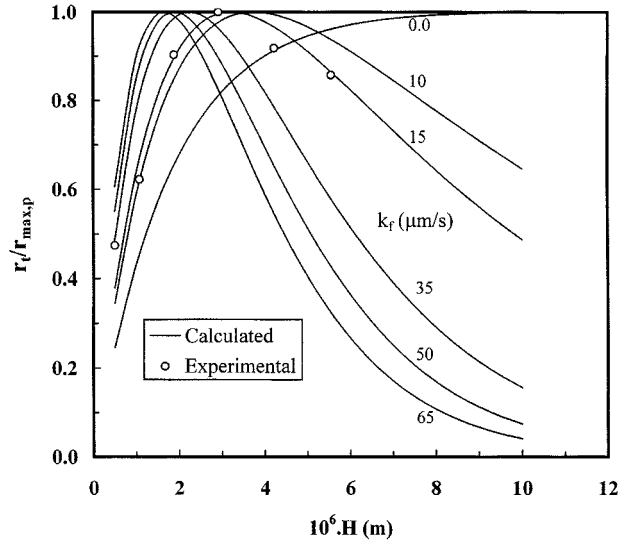

Figure 9. Experimental determination of k_f for SC illumination.

Experimental conditions: $a = 0.89$; $\alpha = 6.264 \times 10^5$ m^{-1}; $D_e = 1.0 \times 10^{-10}$ m^2/s; $A = 0.002$ m^2; $T = 303$ K; $\nu = 1.45 \times 10^{-4}$ m^3; $Re = 427$.

In reality, however, it is impossible to obtain the maximum reaction rate as defined in Eq. 33, because for a given catalyst layer thickness, k_f is never zero. Therefore, we defined a new $r_{max,p}$ for LC illumination by letting $H \to \infty$ and $k_f \neq 0$. From Eq. 32 we get

$$r_{max,p} = \frac{K_d A(1-\epsilon)}{a\alpha + \dfrac{k_f}{D_e}} I_0^a C_b \qquad \text{(LC illumination)}. \quad (38)$$

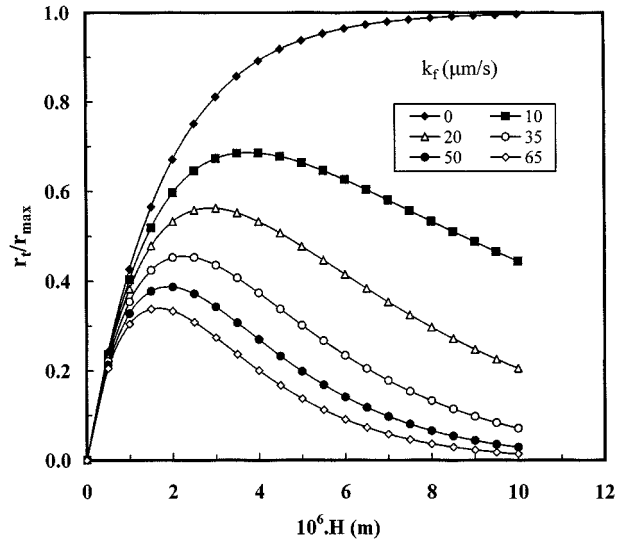

Figure 10. Influence of internal mass transfer on photocatalytic reaction rate for SC illumination.

Experimental conditions: $a = 0.89$; $\alpha = 6.264 \times 10^5$ m^{-1}; $D_e = 1.0 \times 10^{-10}$ m^2/s.

For SC illumination, we can define $r_{max,p}$ by substituting Eq. 36 into Eq. 35:

$$r_{max,p} = \frac{K_d A(1-\epsilon)}{\dfrac{k_f}{D_e} - a\alpha} I_0^a C_b \left\{ \left(\frac{k_f}{a\alpha D_e} \right)^{a\alpha D_e/(a\alpha D_e - k_f)} - \left(\frac{k_f}{a\alpha D_e} \right)^{k_f/(a\alpha D_e - k_f)} \right\} \qquad \text{(SC illumination)}, \quad (39)$$

and accordingly we have

$$\frac{r_t}{r_{max,p}} = 1 - \exp\left[-\left(a\alpha + \frac{k_f}{D_e} \right) H \right] \text{(LC illumination)} \quad (40)$$

$$\frac{r_t}{r_{max,p}} = \frac{\exp(-a\alpha H) - \exp\left(-H \dfrac{k_f}{D_e} \right)}{\left(\dfrac{k_f}{a\alpha D_e} \right)^{a\alpha D_e/(a\alpha D_e - k_f)} - \left(\dfrac{k_f}{a\alpha D_e} \right)^{k_f/(a\alpha D_e - k_f)}} \qquad \text{(SC illumination)}. \quad (41)$$

Experiments were performed for photocatalytic degradation of the benzoic acid using different catalyst layer thicknesses for both SC and LC illumination configurations. Experimental results as well as calculated values of $(r_t/r_{max,p})$ for different k_f values from Eqs. 40 and 41 are shown in Figures 8 and 9, respectively. Experimental results do indeed show that the photocatalytic rate goes through a maximum for SC illumination (Figure 9), while it is constant for LC illumination (Figure 8) when catalyst film is thick. The best k_f values obtaioned when the experimental data were fitted (using the Marquardt method of least-square approximation technique) to the preceding equations are, respectively, 1.48×10^{-5} m/s (LC illumination) and 1.65×10^{-5} m/s (SC illumination). The literature-reported value of k_{rxn} for benzoic acid is 1.145×10^{-4} m/s (Chen, 1999), and therefore is one order of magnitude higher than the k_f values obtained earlier. It should be noted that the overall rate depends on all three rates described in Eq. 1. However, $k_{m,ext}$ can be reduced to significantly lower values by increasing the mixing (or flow rate), and k_{rxn} can be increased somewhat by increasing the light intensity. The internal mass-transfer resistance is difficult to alter, as it depends on the catalyst layer thickness, and one must use thickness at least as close to the optimal value, otherwise the overall rate will decrease.

Conclusions

In this work, the effect of mass transfer and catalyst layer thickness on photocatalytic degradation of benzoic acid over Degussa P25 TiO_2 thin film supported on a Pyrex glass substrate was investigated. A simple illumination source and reactor geometry was used in order to extrapolate the present experimental results for use in the design of a large-scale photocatalytic reactor. Many intriguing advantages exist for immobilized photocatalyst systems over the suspended systems. However, the internal and external mass transfer is one

of the main obstacles for the commercialization of this process. A rational approach, which is also applicable to other photocatalytic systems, was proposed for the determination of external and internal mass-transfer parameters. The experimental results indicate that external mass-transfer resistance could be reduced to a negligible value by increasing the flow rate (Reynolds number) of the solution flowing over the immobilized catalyst. However, the internal mass transfer is an intrinsic property of the catalyst film, and is determined by the nature of the catalyst, coating methods used, and the thickness of the catalyst film. Overall rate is at times controlled by the internal mass-transfer resistance, which is difficult to alter. In this work, dynamic mass-transfer parameters were obtained experimentally to verify a proposed realistic model. Several model parameters, namely, external mass-transfer coefficient, dynamic adsorption equilibrium constant, adsorption rate constant, internal mass-transfer coefficient, and effective diffusivity were determined experimentally using benzoic acid as a model component. All these parameters are extremely important in the design and development of photocatalytic processes, and are not yet available in the literature. Experiments were also conducted to determine the effect of the catalyst layer thickness on the photocatalytic degradation rate for both SC and LC illumination configurations. It was observed that an optimum catalyst layer thickness exists for SC illumination, while the rate reaches a saturation value for LC illumination, and increasing the catalyst layer thickness has no effect on the rate thereafter. The ideal thickness found in this study was around 5 μm. A model was proposed for the dependence of the photocatalytic rate on the catalyst layer thickness, which also predicts the preceding behavior. The internal mass-transfer resistance factor, k_f, obtained was 1.48×10^{-5} m/s for LC illumination and 1.65×10^{-5} m/s for SC illumination.

Notation

R = radius of illuminated window, m
t = time, s
z = axial position, m
ρ = density of catalyst particle, kg/m^3
λ = light wavelength, nm

Subscripts

d = degradation
p = pore

Literature Cited

Bideau, M., B. Claudel, C. Dubien, L. Faure, and H. Kazouan, "On the 'Immobilization' of Titanium Dioxide in the Photocatalytic Oxidation of Spent Waters," *J. Photochem. Photobiol. A: Chem.*, **91**, 137 (1995).

Chen, D. W., and A. K. Ray, "Photodegradation Kinetics of 4-Nitrophenol in TiO_2 Suspension," *Water Res.*, **32**, 3223 (1998).

Chen, D. W., and A. K. Ray, "Photocatalytic Kinetics of Phenol and Its Derivatives over UV Irradiated TiO_2," *Appl. Catal. B: Environ.*, **23**, 143 (1999).

Chen, D. W., "Kinetic Study of Photocatalytic Process for Waterwater Treatment," PhD Thesis, National Univ. of Singapore, Singapore (1999).

Chester, G., M. Anderson, H. Read, and S. Esplugas, "A Jacketed Annular Membrane Photocatalytic Reactor for Wastewater Treatment: Degradation of Formic Acid and Atrazine," *J. Photochem. Photobiol. A: Chem.*, **71**, 291 (1993).

Edwards, M. E., C. M. Villa, C. G. Hill, and T. W. Chapman, "Effectiveness Factors for Photocatalytic Reactions Occurring in Planar Membranes," *Ind. Eng. Chem. Res.*, **35**, 712 (1996).

Fernandez, A., G. Lassaletta, and V. M. Jimenez, "Preparation and Characterization of TiO_2 Photocatalysts Supported on Various Rigid Supports (Glass, Quartz and Stainless Steel). Comparative Studies of Photocatalytic Activity in Water Purification," *Appl. Catal. B: Environ.*, **7**, 49 (1995).

Fox, M. A., and M. T. Dulay, "Heterogeneous Photocatalysis," *Chem. Rev.*, **93**, 341 (1993).

Froment, G. F., and K. B. Bischoff, *Chemical Reactor Analysis and Design*, Wiley, New York (1990).

Haarstrick, A., O. M. Kut, and E. Heinzle, "TiO_2-Assisted Degradation of Environmentally Relevant Organic Compounds in Wastewater Using a Novel Fluidized Bed Photoreactor," *Environ. Sci. Technol.*, **30**, 817 (1996).

Hoffmann, M. R., S. T. Martin, W. Choi, and D. W. Bahnemann, "Environmental Applications of Semiconductor Photocatalysis," *Chem. Rev.*, **95**, 69 (1995).

Hofstadler, K., R. Bauer, S. Novalic, and G. Heisler, "New Reactor Design for Photocatalytic Wastewater Treatment with TiO_2 Immobilized on Fused-Silica Glass Fibers: Photomineralization of 4-Chlorophenol," *Environ. Sci. Technol.*, **28**, 670 (1994).

Ichikawa, S., and R. Doi, "Photocatalytic Degradation of Malonic Acid in Aqueous Suspensions of TiO_2: An Initial Kinetic Investigation of CO_2 Photogeneration," *Catal. Today*, **27**, 271 (1996).

Legrini, O., E. Oliveros, and A. M. Braun, "Photochemical Processes for Water Treatment," *Chem. Rev.*, **93**, 671 (1993).

Lu, M. C., G. D. Roam, J. N. Chen, and C. P. Huang, "Factors Affecting the Photocatalytic Degradation of Dichlorvos over Titanium Dioxide Supported on Glass," *J. Photochem. Photobiol. A: Chem.*, **76**, 103 (1993).

Matthews, R. W., "Photooxidation of Organic Impurities in Water Using Thin Films of Titanium Dioxide," *J. Phys. Chem.*, **91**, 3328 (1987).

Matthews, R. W., and S. R. McEvoy, "Photocatalytic Degradation of Phenol in the Presence of Near-UV Illuminated Titanium Dioxide," *J. Photochem. Photobiol. A: Chem.*, **64**, 231 (1992).

Matthews, R. W., "Photocatalytic Oxidation of Organic Contaminants in Water: An Aid to Environmental Preservation," *Pure Appl. Chem.*, **9**, 1285 (1992).

Miller, R., and R. Fox, *Photocatalytic Purification and Treatment of Water and Air*, D. F. Ollis and H. Al-Ekabi, eds., Elsevier, Amsterdam, p. 573 (1993).

Mills, A., R. Davies, and D. Worsley, "Water Purification by Semiconductor Photocatalysis," *Chem. Soc. Rev.*, **22**, 417 (1993).

Mills, A., and S. L. Hunte, "An Overview of Semiconductor Photocatalysis," *J. Photochem. Photobiol. A: Chem.*, **108**, 1 (1997).

Mukherjee, P. S., and A. K. Ray, "Major Challenges in the Design of a Large-Scale Photocatalytic Reaction for Water Treatment," *Chem. Eng. Technol.*, **22**, 253 (1999).

Nogueira, F. P. R., and W. F. Jardim, "TiO_2-Fixed-Bed Reactor for Water Decontamination Using Solar Energy," *Sol. Energy*, **56**, 471 (1996).

Ollis, D. F., E. Pelizzetti, and N. Serpone, *Photocatalysis: Fundamentals and Applications*, N. Serpone and E. Pelizzetti, eds., Wiley Interscience, New York, p. 603 (1989).

Ollis, D. F., E. Pelizzetti, and N. Serpone, "Destruction of Water Contaminants," *Environ. Sci. Technol.*, **25**, 1523 (1991).

Ollis, D. F., and H. Al-Ekabi, eds., *Photocatalytic Purification and Treatment of Water and Air*, Elsevier, Amsterdam (1993).

Patankar, S. V., *Numerical Heat Transfer and Fluid Flow*, McGraw-Hill, New York (1980).

Peill, N. J., and M. R. Hoffmann, "Chemical and Physical Characterization of a TiO_2-Coated Fiber Optic Cable Reactor," *Environ. Sci. Technol.*, **30**, 2806 (1996).

Periyathamby, U., and A. K. Ray, "Computer Simulation of a Novel Photocatalytic Reactor Using Distributive Computing," *Chem. Eng. Technol.* **22**(10), 881 (1999).

Ray, A. K., and A. A. C. M. Beenackers, "A Photocatalytic Reactor Suitable for Water Purification as Well as a Process for the Purification of Waste Water by Means of Such a Photocatalytic Reactor," European patent No. 96200942.9-2104 (1996).

Ray, A. K., and A. A. C. M. Beenackers, "Novel Swirl-Flow Reactor

for Kinetic Studies of Semiconductor Photocatalysis,'' *AIChE J*., **43**, 2571 (1997).
Ray, A. K., and A. A. C. M. Beenackers, ''Novel Photocatalytic Reactor for Water Purification,'' *AIChE J*., **44**, 477 (1998a).
Ray, A. K., and A. A. C. M. Beenackers, ''Development of a New Photocatalytic Reactor for Water Purification,'' *Catal. Today*, **40**, 73 (1998b).
Ray, A. K., ''Design Development and Experimentation of a New Photocatalytic Reactor for Water Treatment,'' *Chem. Eng. Sci*., **54**, 3113 (1999).
Sabate, J., M. A. Anderson, H. Kikkawa, M. Edwards, and C. G. Hill, ''A Kinetic Study of the Photocatalytic Oxidation of 3-Chlorosalicylic Acid over TiO_2 Membrane Supported on Glass,'' *J. Catal*., **127**, 167 (1991).
Schiavello, M., ed., *Photocatalysis and Environment: Trends and Applications*, Kluwer, Dordrecht (1988).
Sclafani, A., A. Brucato, and L. Rizzuti, *Photocatalytic Purification and Treatment of Water and Air*, D. F. Ollis and H. Al-Ekabi, eds., Elsevier, Amsterdam, p. 533 (1993).
Serpone, N., E. Borgarello, R. Harris, P. Cahill, M. Borgarello, and E. Pelizzetti, ''Photocatalysis over TiO_2 Supported on a Glass Substrate,'' *Sol. Energy Mater*., **14**, 121 (1986).
Serpone, N., and E. Pelizzetti, eds., *Photocatalysis, Fundamentals and Applications*, Wiley, New York (1989).
Sodergren, S., A. Hagfeldt, J. Olsson, and S. E. Lindquist, ''Theoretical-Models for the Action Spectrum and the Current-Voltage Characteristics of Microporous Semiconductor-Films in Photoelectrochemical Cells,'' *J. Phys. Chem*., **98**, 5552 (1994).
Tennakone, K., and I. R. M. Kottegoda, ''Photocatalytic Mineralization of Paraquat Dissolved in Water by TiO_2 Supported on Polythene and Polypropylene Films,'' *J. Photochem. Photobiol. A: Chem*., **93**, 79 (1996).
Torimoto, T., S. Ito, S. Kuwabata, and H. Yoneyama, ''Effects of Absorbents Used as Supports for Titanium Dioxide Loading on Photocatalytic Degradation of Propyzamide,'' *Environ. Sci. Technol*., **30**, 1275 (1996).
Vinodgopal, K., S. Hotchandani, and P. V. Kamat, ''Electrochemically Assisted Photocatalysis: TiO_2 Particulate Film Electrodes for Photocatalytic Degradation of 4-Chlorophenol,'' *J. Phys. Chem*., **97**, 9040 (1993).
Zhang, Y., J. C. Crittenden, D. W. Hand, and D. L. Perram, ''Fixed-Bed Photocatalysts for Solar Decontamination of Water,'' *Environ. Sci. Technol*., **28**, 435 (1994).

Manuscript received July 21, 1999, and revision received Nov. 29, 1999.